

Canard explosions in turbulent thermo-fluid systems

Ramesh S. Bhavi,^{1,2, a)} Sivakumar Sudarsanan,^{1,2} Manikandan Raghunathan,^{1,2}
Anaswara Bhaskaran,^{1,2} and R. I. Sujith^{1,2}

¹⁾*Department of Aerospace Engineering, Indian Institute of Technology Madras, Chennai, Tamil Nadu 600036, India.*

²⁾*Centre of Excellence for Studying Critical Transition in Complex Systems, Indian Institute of Technology Madras, Chennai, Tamil Nadu 600036, India.*

(Dated: 14 June 2024)

A sudden transition to a state of high amplitude limit cycle oscillations is catastrophic in a thermo-fluid system. Conventionally, upon varying the control parameter, a sudden transition is observed as an abrupt jump in the amplitude of the fluctuations in these systems. In contrast, we present an experimental discovery of a canard explosion in a turbulent reactive flow system where we observe a continuous bifurcation with a rapid rise in the amplitude of the fluctuations within a narrow range of control parameters. The observed transition is facilitated via a state of bursting, consisting of the epochs of large amplitude periodic oscillations amidst the epochs of low amplitude periodic oscillations. The amplitude of the bursts is higher than the amplitude of the bursts of intermittency state in a conventional gradual transition, as reported in turbulent reactive flow systems. During the bursting state, we observe that temperature fluctuations of exhaust gas vary at a slower time scale in correlation with the amplitude envelope of the bursts. We also present a phenomenological model for thermoacoustic systems to describe the observed canard explosion. Using the model, we explain that the large amplitude bursts occur due to the slow-fast dynamics at the bifurcation regime of the canard explosion.

^{a)}Electronic mail: rameshbhavi003@gmail.com

Transition to oscillatory instabilities in turbulent reactive flow systems is a long pending issue in designing modern combustors of engines that have high-power ratings. Nonlinear interactions between the hydrodynamic flow field, the acoustic field and the heat-release rate fluctuations in a confined environment make a turbulent combustor a complex dynamical system. The state of these systems changes from a stable operation to a state of oscillatory instability as the control parameter is varied. In turbulent combustors, past studies were focused on the gradual transitions to the state of oscillatory instability via the state of intermittency. Most recently, the discovery of abrupt transitions in turbulent reactive flow systems has been a highlight, which is a contrasting scenario of a gradual transition. Abrupt transitions are sudden and discontinuous in nature. However, in this study, we report the discovery of a canard explosion, which is a transition involving a rapid rise in the amplitude of the oscillations but continuous in nature. Canard explosions are characterized by the amplitude of the oscillations reaching a very high value within a narrow range of control parameters. Further, we also observe that the transition is facilitated via the state of bursting, where the bursts are of large amplitude. We show that such bursts are possible when there is a fluctuation in the parameter at the bifurcation regime of the underlying canard explosion.

I. INTRODUCTION

Emergent oscillatory instabilities are well-known in fluid mechanical systems. Such instabilities are observed in thermoacoustic¹, aeroacoustic², and aeroelastic systems³. The state of oscillatory instabilities corresponds to the unstable operation in many such systems. The large amplitude oscillations during the state of instability hamper healthy working conditions of these engineering systems, consequently leading to catastrophic failures⁴⁻⁶. These oscillatory instabilities arise due to the nonlinear interactions between the sub-systems of a fluid mechanical system, as a control parameter is changed.

The transition from a stable operation to an unstable operation in a dynamical system is referred to as a bifurcation to the state of limit cycle oscillations (LCO)^{7,8}. In laminar

thermo-fluid systems, where the dynamics of the flow is calm and quiet, the transition is a Hopf-bifurcation as the system transits from a silent state (fixed point) to an oscillatory state^{9,10}. In the case of turbulent systems, the dynamics comprise vigorous turbulent fluctuations in the flow. In these turbulent systems, the stable operation is characterized by chaotic oscillations¹¹, and the unstable operation corresponds to an ordered state of periodic oscillations¹². Studies in the recent decade have shown that the state of intermittency, an asymptotic state which has the imprints of chaos and order, presages the emergence of order¹³. The emergence of order via the state of intermittency is predominantly observed as a gradual change in the root mean square (RMS) value, a statistical measure of acoustic pressure oscillations. Hence, in turbulent systems, the bifurcation is viewed as a gradual emergence of order from the state of chaos^{12,14}. In contrast to the gradual transition via the state of intermittency, recently, abrupt transitions to the state of order have also been discovered in turbulent systems¹⁵⁻¹⁷. In abrupt transition, a sudden discontinuous jump in the RMS of the acoustic pressure oscillations is observed.

Abrupt transitions are also referred to as explosive transitions and are characterized by the phenomenon of hysteresis¹⁸. The occurrence of hysteresis is due to the simultaneous presence of multiple stable regimes for a range of control parameters^{16,19}. However, in practical engineering systems, there are exceptions where a genuine abrupt rise in the statistical measure of the oscillations is observed, but the transition is not discontinuous²⁰. Such transitions, where a rapid rise in the amplitude of the fluctuation occurs for a minute increment in the control parameter, were primarily investigated in the Van der Pol oscillator model and are referred to as canard explosions²¹. Canard explosions have been reported in many real-world systems such as chemical oscillations²⁰, ground dynamics of an aircraft²², neuronal activity²³, predator-prey food chains²⁴, and light emitting diodes²⁵.

In a transition involving a canard explosion, the amplitude of the limit cycle grows significantly soon after the Hopf bifurcation²⁶. The dynamics of the system during a canard explosion becomes highly sensitive to variation in the control parameter. There is a significant growth in the amplitude of the oscillation for an exponentially small range of values of the control parameter at the canard explosion regime²⁰. Hence, a canard explosion appears abrupt if there is a lack of resolution in the variation in system parameters²⁷. A continuous transition comprising a canard explosion, albeit appears abrupt, traces the same forward and reverse path in the control parameter variation²⁶. Further, large amplitude bursts and

mixed-mode oscillations are observed when the system exhibits slow-fast dynamics at the canard explosion regime^{28,29}.

Here, we report the observation of canard explosions in thermo-fluid systems for the first time, to the best of our knowledge. We present the experimental results for the rapid rise in amplitude of the acoustic pressure oscillations within a minute range of the control parameter, a principal feature of the canard explosion. The transition is continuous in nature and exhibits no hysteresis. We also observe a bursting behaviour comprising the bursts of large amplitude acoustic pressure oscillations near the canard explosion regime. Through experimentally measuring the exhaust gas temperature during the state of bursting, we show that a system parameter fluctuates at a time scale slower than the system oscillations. Further, we describe the observed transition of canard explosion using a low-order thermoacoustic model. Using the low-order model, we attribute the bursting behaviour during the canard explosion to a coupling between a slow oscillatory term and the driving term.

The rest of the paper is organized as follows: Section II provides a detailed description of the experiments and the setups used in this study. The experimental results of the transitions involving canard explosions are described in Section III. The low-order thermoacoustic model describing canard explosions is presented in Section IV, and the mechanism of large amplitude bursting dynamics is illustrated in Section IV A. Section V narrates the conclusions of the study.

II. EXPERIMENTS

In order to check the commonality of the transition to oscillatory instabilities in different turbulent reactive flow systems, we conducted experiments in three different configurations of combustors. These systems function in turbulent conditions and represent the dynamics of combustors in modern gas turbines and rocket engines. The details of the combustor setups are discussed below.

A. Dump combustor configurations

Figure 1(a) represents the experimental setup for the dump combustor. A fluid mixture of compressed air and liquid petroleum gas (60% Propane & 40% butane) is used for chemical

reactions in a combustion chamber. The combustion chamber is 1100 mm long and has a $90 \times 90 \text{ mm}^2$ square cross-section. The setup has three main sections along the fluid flow—a plenum chamber, a burner, and the combustion chamber. The air enters the combustor via a flow equalization chamber referred to as a plenum chamber, which helps isolate the combustion chamber from the fluctuations upstream of the flow. The fuel is injected in the burner section between the plenum chamber and the combustion chamber, where the fuel and the air are premixed. The diameter of the burner is 40 mm. The fuel-air mixture enters the combustion chamber at the dump plane, where there is a sudden increase in the cross-sectional area from the burner to the combustion chamber. The exit of the combustion chamber is connected to a large rectangular box referred to as a decoupler. The dimensions of the decoupler are set to be much larger than the cross-sectional dimensions of the combustion chamber. The utility of the decoupler is to reduce sound emissions from the combustion chamber³⁰.

The dynamics of the system is studied by varying the equivalence ratio ϕ as the control parameter. The equivalence ratio is defined as $\phi = \Upsilon_{\text{actual}}/\Upsilon_{\text{stoichiometric}}$, where Υ is the ratio of the mass flow rate of the fuel and the air. Thus, ϕ is a function of air and fuel flow rates, which are controlled using mass flow controllers (MFC). The uncertainty in the flow rate measurement is $\pm(0.8 \%$ of the reading $+ 0.2 \%$ of the full scale). The uncertainty in the computed value of ϕ is $\pm 2\%$. The control parameter (ϕ) is varied in a quasi-static manner. The qualitative change in the behaviour of the system is analyzed by measuring the acoustic pressure fluctuations in the combustion chamber. We used Piezoelectric pressure transducers (PCB103B02) for measuring the acoustic field fluctuations. The sensitivity of the transducers is 217.5 mV/kPa. We acquire the signal from the pressure transducer for 5 s at a sampling rate of 10 kHz after an initial waiting time of 3 s at each set point of the control parameter. The maximum uncertainty in the measured values of the pressure signal is $\pm 0.15 \text{ Pa}$. The experiments were performed in two different configurations of the dump combustor, which will be detailed in the following subsections.

1. Dump combustor with a swirler configuration

A swirler (refer to Fig. 1b), inducing swirl motion to the flow, is used at the entry of the combustion chamber. The swirling motion aids in the establishment of the flame in a

compact form, stretching over a small section of the combustion chamber. The diameter (d) of the swirler is 40 mm. The swirler consists of 8 vanes, with each vane having an angle of 40° with respect to the direction of the bulk flow in the combustor. The location of the swirler is such that the front part of each vane is 20 mm from the dump plane. In this swirler configuration, we maintain a constant fuel flow rate of 28 standard litres per minute (SLPM). The equivalence ratio varies from 0.783 to 0.532 by increasing the airflow rate from 800 SLPM to 1436 SLPM. The Reynolds number for the system, based on the diameter of the swirler, changes between $Re_d = 2.76 \times 10^4 \pm 220$ and $4.94 \times 10^4 \pm 220$. A K-type thermocouple is used to measure the temperature of the hot gases downstream of the flow. The signal for the temperature was acquired for 5 s at a sampling rate of 20 Hz.

2. Dump combustor with a bluff body configuration

In this configuration of the dump combustor, we replace the earlier flame holder (swirler) with a bluff body (refer to 1c). A bluff body slows the flow by creating a flow re-circulation zone, providing sufficient time for the air-fuel mixture to react in a compact zone of the combustion chamber³¹. The bluff body is located at a distance of 27.5 mm from the dump plane of the combustion chamber. The diameter (d) of the bluff body is 47 mm. The fuel for the combustor is introduced in the burner at a distance of 85 mm from the dump plane, through the hollow shaft anchoring the bluff body. We maintain a constant fuel flow rate of 42 SLPM in this bluff body configuration. The equivalence ratio varies from 1.909 to 1.022 by increasing the airflow rate from 600 SLPM to 1200 SLPM. The corresponding Reynolds number, computed based on the diameter of the bluff body, changes in the range of $Re_d = 1.76 \times 10^4 \pm 220$ to $3.28 \times 10^4 \pm 220$.

B. Annular combustor

Figure 1(d) represents a swirl-stabilized annular combustor, where sixteen flames from the circumferentially arranged burners are established during the experiments. Premixed air and LPG are used for chemical reactions. The air and the fuel initially enter a premixing chamber through an air/fuel inlet. The premixed mixture then enters into a flow-settling chamber. We incorporate a honeycomb-like structure inside the settling chamber to render

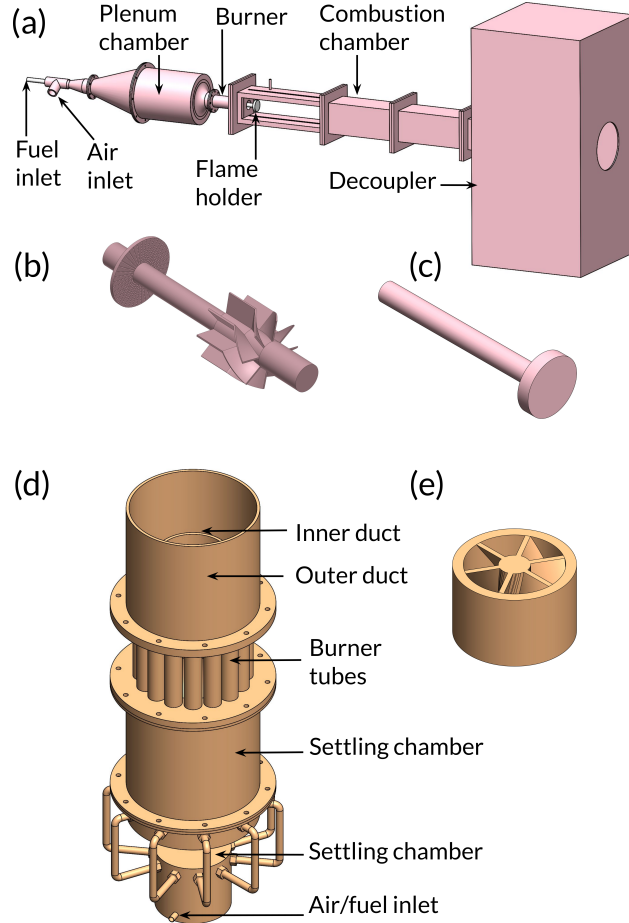


FIG. 1. Schematic of (a) a dump combustor which can be operated in two different configurations based on the flame holding mechanisms. We use (b) the swirler and (c) the bluff body as two different flame holders for the dump combustor. Schematic of (d) the annular combustor comprising sixteen burners. At the exit of each burner, (e) a swirler is used as a flame holder.

the flow in one direction. The flow through the settling chamber encounters a hemispherical flow divider that uniformly distributes the fuel-air mixtures to the 16 burner tubes. The burner tubes exit into the combustion chamber comprising an outer and inner cylindrical duct. The chemical reactions are individually established in the annulus of the outer and the inner cylindrical duct after passing through the swirler fitted at the exit of each burner tube. The swirlers consist of vanes which are inclined at an angle of $\beta = 60^\circ$ with the axial flow direction (refer to Fig. 1e). The burner tubes are 300 mm long and have a circular cross-section (30 mm diameter). The diameter of the inner and the outer cylindrical ducts are 400 mm and 300 mm, respectively. The length of the inner and the outer cylindrical

ducts are 510 mm and 140 mm, respectively.

The equivalence ratio (ϕ) is varied from 1.4 to 0.9 in a quasi-static manner by varying the fuel flow rate. The airflow rate is kept constant at 1800 SLPM throughout the experiments. The fuel flow rate is varied from 92 to 59 SLPM. The Reynolds number, calculated using the exit diameter of the burner, is $Re_d \approx 1.01 \times 10^4 \pm 220$. The dynamics of the system is analyzed by measuring the acoustic pressure fluctuations from the combustion chamber. Piezoelectric pressure transducers (PCB103B02) of sensitivity 217.5 mV/kPa are used for pressure fluctuation measurements. The pressure signal at each control parameter is acquired for 5 s at a sampling rate of 10 kHz after an initial waiting time of 3 s at each set point of the control parameter. A K-type thermocouple is used to measure the temperature of the hot gases downstream of the flow.

III. CANARD EXPLOSIONS IN TURBULENT COMBUSTORS

Figure 2 represents the bifurcation diagram and the nature of the sudden transition in the bluff body stabilized dump combustor. In order to study the sudden transitions via canard explosions, we varied the equivalence ratio (ϕ) as the control parameter. Initially, when the airflow rate is varied in steps of 30 SLPM, we observed an abrupt transition (refer to points d and e in Fig. 2a). The abrupt transition is from low amplitude ($p'_{\text{rms}} = 420$ Pa) to high amplitude ($p'_{\text{rms}} = 3525$ Pa) acoustic pressure fluctuations. Here, p'_{rms} represents the root mean square value of the acoustic pressure fluctuations (p'). The corresponding time series are presented in Fig. 2(d, e). To further investigate this seemingly abrupt transition, we varied the airflow rate at finer steps (10 SLPM) between the points of the control parameter corresponding to the abrupt jump. A continuous, albeit steep, variation in the RMS value of the p' is observed when the control parameter is varied in finer steps (refer to Fig. 2b). We further note that the continuous transition occurs via a state of bursting (refer to Fig. 2f-i). During the state of bursting, we observe large amplitude fluctuations ($p' \approx 3500$ Pa) amidst low amplitude fluctuations ($p' \approx 500$ Pa) (refer to Fig. 2g).

Further, when the control parameter is varied in the reverse direction, the transition retraces the forward path (refer to Fig. 2c). Similar observations of the canard explosions were observed when we performed experiments in a swirl-stabilized dump combustor (Fig 3). In the swirl-stabilized dump combustor, as the equivalence ratio is decreased from 0.783 to

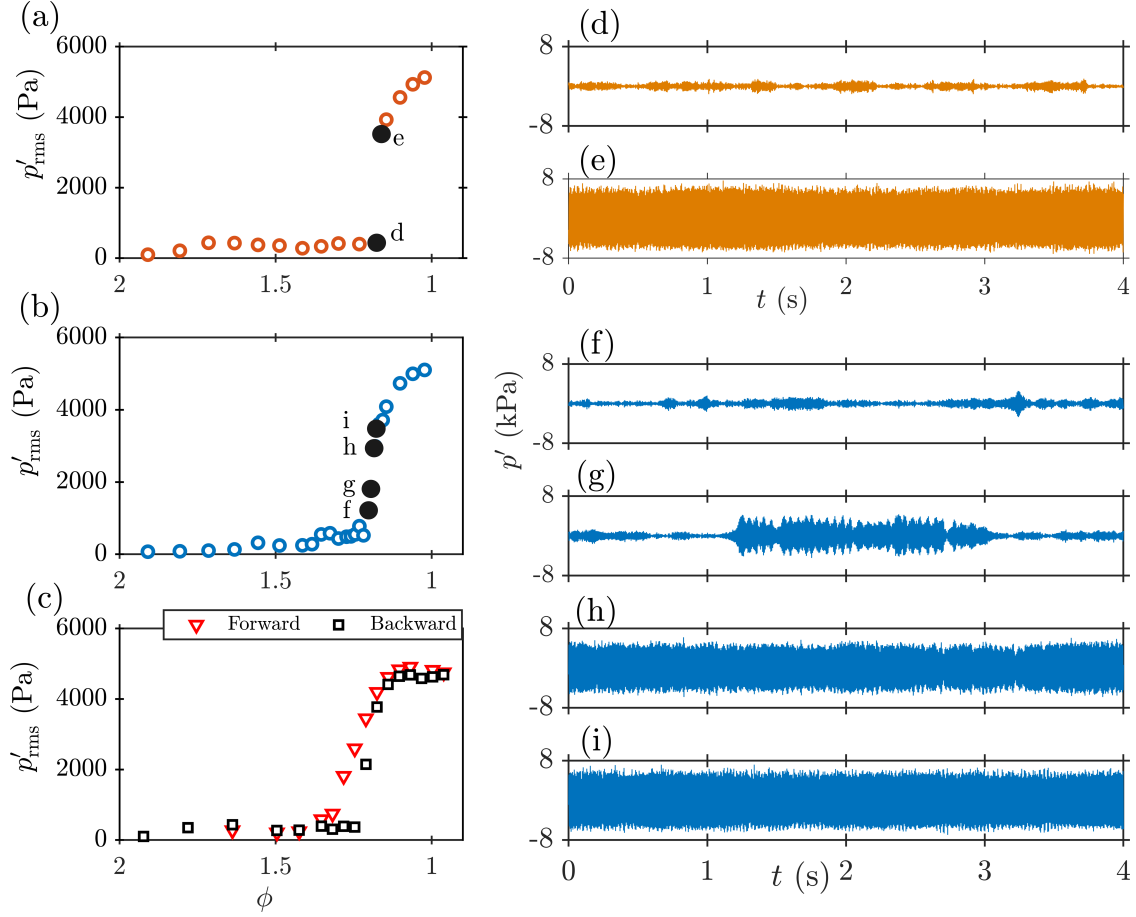


FIG. 2. Representation of a sudden transition to high amplitude limit cycle oscillations via canard explosion in the bluff body stabilized dump combustor. **(a,b & c)** The bifurcation diagrams for the variation of the RMS value of the acoustic pressure fluctuations (p'_{rms}) as a function of the equivalence ratio ϕ . **(d-i)** The corresponding time series of the acoustic pressure signal during canard explosion. **(a)** Sudden transition from a low amplitude **(d)** ($p'_{\text{rms}} = 420$ Pa) to very high amplitude **(e)** ($p'_{\text{rms}} = 3525$ Pa) acoustic pressure fluctuations as ϕ is varied. When ϕ is varied in finer steps between these apparently abrupt transition points, we observe a **(b)** continuous transition **(f-i)** to high amplitude fluctuations via **(g)** bursting dynamics. **(c)** The transition retraces the forward path when ϕ is varied in the reverse direction, implying the absence of the hysteresis. Thus, we observe a transition with a rapid rise in the amplitude of acoustic pressure fluctuations at a certain value of the control parameter.

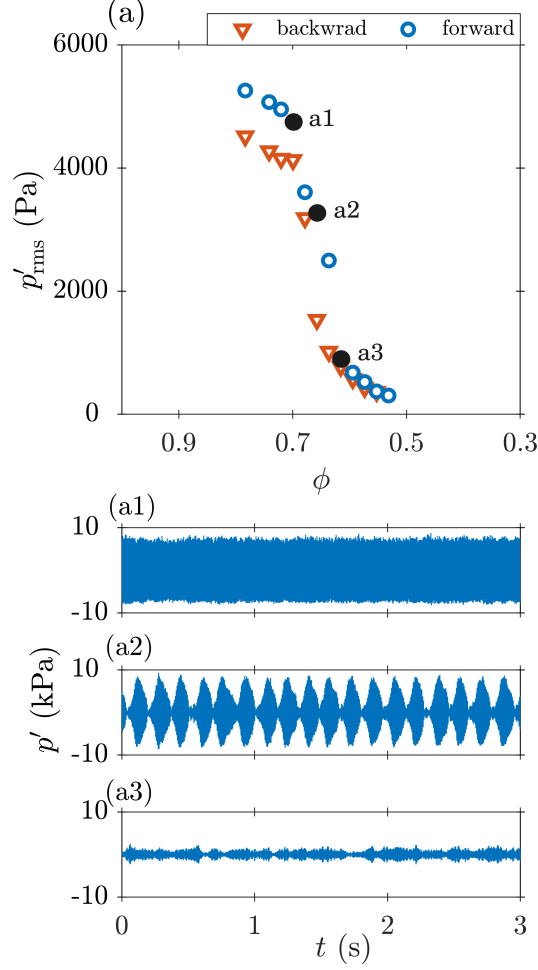


FIG. 3. Representation of the sudden transition via canard explosion in a swirl stabilized dump combustor. **(a)** The forward and reverse path of the transition via the canard explosion. The equivalence ratio (ϕ) in the forward path is varied from 0.783 to 0.532. We notice that the transition occurs via the state of large amplitude bursting **(a1-a3)**.

0.532, we observe a rapid decrease in the variation of RMS value of the acoustic pressure fluctuations (refer to the points a1, a2, & a3 of Fig. 3a). The transition is from a state of high amplitude fluctuations ($p'_{\text{rms}} = 4730$ Pa) to a state of low amplitude fluctuations ($p'_{\text{rms}} = 770$ Pa) (refer to Fig. 3a1, a3). Additionally, we note that when the parameter is varied in the reverse direction, the system retraces the forward path (Fig. 3a). The difference in the values of p'_{rms} at the state of thermoacoustic instability in forward and reverse paths is due to increased damping as a result of prolonged heating of the combustor walls³². Thus, we note that a continuous but steep transition involving a canard explosion exhibits no hysteresis.

Further, in the swirl stabilized dump combustor, the steep rise in RMS value of p' to a

high amplitude oscillatory instability occurs via the state of large amplitude bursting (refer to point a2 in Fig. 3a). The state of bursting has imprints corresponding to the states of low-amplitude fluctuations and high-amplitude fluctuations (Fig. 3a2 & a1). Similarly, when ϕ is varied from 1.4 to 0.9 in an annular combustor, we observe a sudden transition for $\phi > 1.075$ (refer to Fig. 4a). Upon varying ϕ in the reverse direction, the transition retraces its path. Moreover, we note that the transition occurs via a state of large amplitude bursting (refer to Fig. 4b2). The bursting state has the imprints of low-amplitude fluctuations and high-amplitude fluctuations (cf. ref Fig. 4b1, b2 & b3), similar to the bursting characteristics observed in the swirl stabilized dump combustor. However, the time interval of bursting oscillations in the annular combustor is larger than the time interval of bursting in the swirl-stabilized combustor. In summary, in all three combustors, we observe that the amplitude of the bursts corresponding to an underlying canard explosion is very high due to the rapid nature of the transition at the bifurcation regime.

In order to investigate the bursting phenomenon, we experimentally measure temperature fluctuations of the hot exhaust gases for the swirl-stabilized dump combustor during the state of bursting ($\phi = 0.657$). The temperature fluctuations are measured using a K-type thermocouple. The exhaust gas temperature is governed by the internal variables of the combustor, such as flame temperature, equivalence ratio and the heat transfer rate to the combustor walls. These variables, in turn, govern the dynamics of the oscillatory instabilities exhibited by a combustor.

Figure 5 represents the variation in temperature alongside the acoustic pressure fluctuation p' during bursting in a swirl stabilized dump combustor. We note that there is a strong correlation between the temperature fluctuation (T') and the envelope of the bursting oscillations (p'_{env}). The strength of the correlation is tested by computing Pearson's correlation coefficient (r), and the value of r is 0.84 for T' and p'_{env} . The time series of T' is band passed to remove the fluctuations lesser than 1 Hz for computing the value of r . Moreover, the local maxima of T' are in the high amplitude bursting regime of p' , and the local minima of T' are in the low amplitude regime of p' (Fig. 5a). This rhythmic variation of T' and p'_{env} is also evident in the amplitude spectrum of the envelope of acoustic pressure fluctuations (\hat{p}'_{env}) and the temperature fluctuations (\hat{T}'_{env}) having the same dominant frequency at 6 Hz (refer to Fig. 5b,c). A similar observation of variation in T' and the envelope of p' , but out of phase pattern, is made for the state of large amplitude bursting in the annular combustor

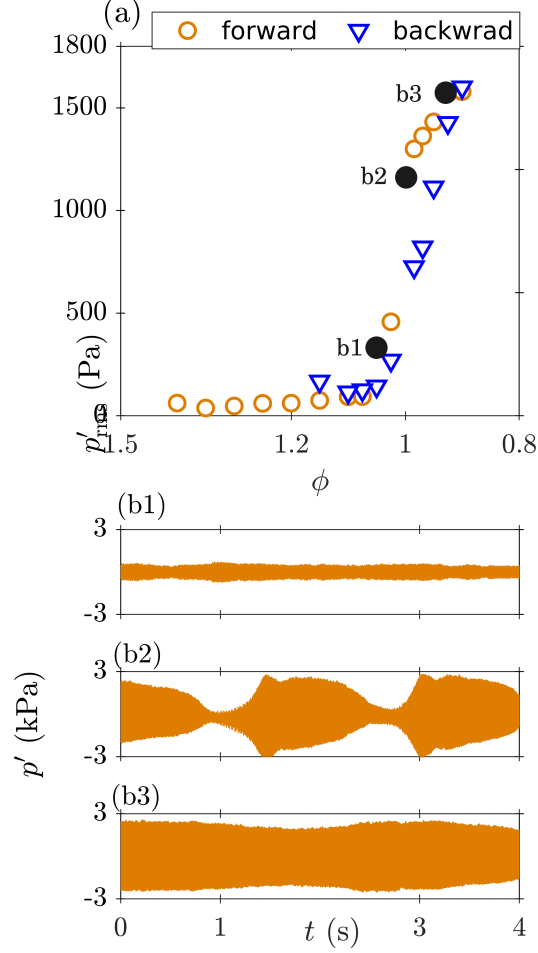


FIG. 4. Representation of the sudden transition via canard explosion in an annular combustor. (a) The forward and reverse path of the transition via the canard explosion. The equivalence ratio (ϕ) in the forward path is varied from 1.4 to 0.9. We notice that the transition occurs via the state of large amplitude bursting (**b1-b3**).

at $\phi = 1$ (refer to Fig. 5d).

Further, the past literature on bursting dynamics suggests that bursting occurs when a system parameter fluctuates at a slower time scale at the bifurcation regime^{33–35}. Therefore, observing variation in temperature fluctuations in correlation with the bursting amplitude (Fig. 5), we note that a system parameter is fluctuating at a slower time scale at the bifurcation regime.

Thus, it is evident from Figs. 2, 3 and 4 that sudden transitions via canard explosions occur in three different turbulent reactive flow systems. Despite differences in the nature of the flow fields and the flame acoustic interactions in these different turbulent combustor

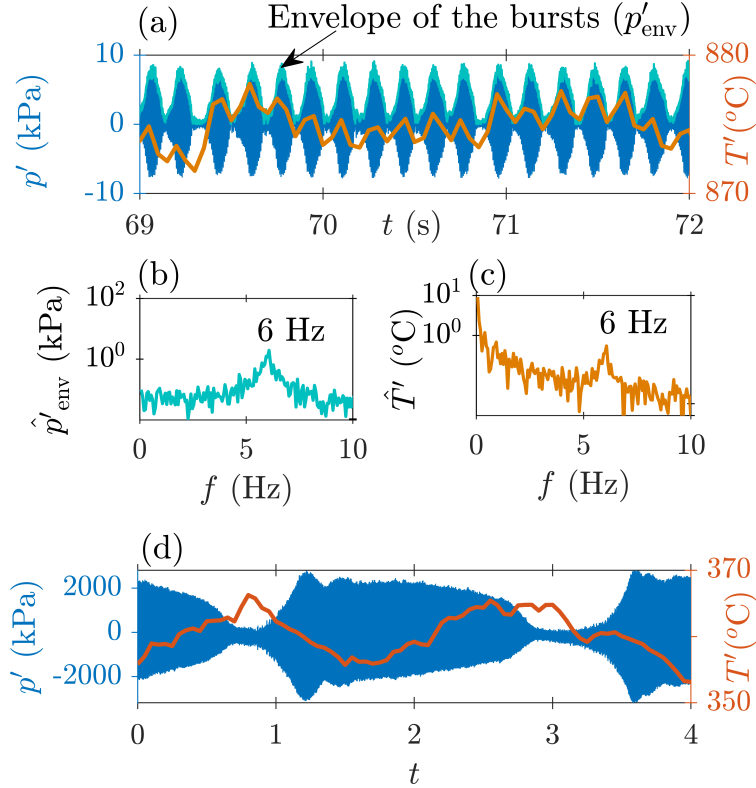


FIG. 5. (a) Representation of the variation of the exhaust gas temperature (T') along with the acoustic pressure fluctuations (p') for a swirl stabilized dump combustor, measured during the state of bursting via canard explosions ($\phi = 0.657$). (b-c) The amplitude spectrum of the envelope of acoustic pressure fluctuations (\hat{p}'_{env}) and the temperature fluctuations (\hat{T}'_{env}) have the same dominant frequency at 6 Hz. (d) The variation of T' along with p' for an annular combustor, measured during the state of bursting via canard explosions ($\phi = 1$). Notice the pattern of variations in T' and the envelope of the p' ; the maxima of T' is in the region of minimum p' , and the minima of T' is in the region of maximum p' .

configurations, we observe a common transition via canard explosion. The observation of large amplitude bursts in the regime of bifurcation hints towards an underlying universal mechanism, which we illustrate in the following subsections using a low-order model for thermo-fluid systems. Motivated by these results, we consider a modified Van der Pol oscillator as illustrated by Ananthkrishnan *et al.*³⁶ to describe the sudden transition. We reduce the influence of the lower-order nonlinearities such that the variation of the system amplitude becomes highly sensitive to the control parameter at the bifurcation regime. We further incorporate a slowly varying coupling term to the acoustic driving to obtain the

phenomenon of large amplitude bursting.

IV. MODELLING CANARD EXPLOSION IN THERMOACOUSTIC SYSTEM

The dynamics of the canard explosion presented in the above experiments is mainly associated with the change in the amplitude of the acoustic pressure fluctuations as the parameter is varied. Since we are concerned with modelling the rapid continuous rise in the amplitude, the thermoacoustic system considered here is one-dimensional, where the axial modes are excited. The effects of mean flow and temperature gradient are neglected^{37,38}. The nonlinear acoustic terms are considered insignificant as the pressure fluctuations relative to the mean are negligible. Thus, the dynamics of the acoustic pressure and the heat release rate fluctuations inside the combustion chamber is governed by the linearized momentum and energy conservation equations³⁸, which are given as,

$$\frac{1}{\bar{\rho}} \frac{\partial p'(z, t)}{\partial z} + \frac{\partial u'(z, t)}{\partial t} = 0, \quad (1)$$

$$\frac{\partial p'(z, t)}{\partial t} + \gamma \bar{p} \frac{\partial u'(z, t)}{\partial z} = (\gamma - 1) \dot{Q}'(z, t) \delta(z - z_f). \quad (2)$$

Here, t is time, z is the distance along the axial direction of the duct, and γ is the specific heat ratio. $\bar{\rho}$ and \bar{p} indicate the mean density and pressure, while p' and u' are the pressure and velocity fluctuations, respectively. We assume the chemical reaction zone to be of a smaller volume such that the heat release rate fluctuations \dot{Q}' are concentrated at a location z_f , which is represented by a Dirac-delta (δ) function³⁹. Equations (1) and (2) can be appropriately modified to obtain an inhomogeneous wave equation, as given below⁴⁰:

$$\begin{aligned} & c^2 \frac{\partial^2 p'(z, t)}{\partial z^2} - \frac{\partial^2 p'(z, t)}{\partial t^2} \\ & = -(\gamma - 1) \frac{\partial \dot{Q}'(z, t)}{\partial t} \delta(z - z_f), \end{aligned} \quad (3)$$

where, $c = \sqrt{\gamma \bar{p} / \bar{\rho}}$ is the speed of sound. We obtain an ordinary differential equation by simplifying Eq. (3) using a Galerkin modal expansion⁴¹. The u' and p' are projected on a set of spatial basis functions (sines and cosines). The temporal coefficients of the basis

functions are η and $\dot{\eta}$, and are represented as:

$$\begin{aligned} p'(z, t) &= \bar{p} \sum_{j=1}^n \frac{\dot{\eta}_j(t)}{\omega_j} \cos(k_j z) \quad \text{and} \\ u'(z, t) &= \frac{\bar{p}}{\bar{\rho}c} \sum_{j=1}^n \eta_j(t) \sin(k_j z), \end{aligned} \quad (4)$$

where j represent the eigenmodes. The basis functions satisfy the acoustic boundary conditions—i.e., $u' = 0$ at the closed end and $p' = 0$ at the open end of the duct. The chosen basis functions are orthogonal in nature. These basis functions also form the eigenmodes of the self-adjoint part of the linearized equations³⁸. Here, for a given length of the combustor L , k_j is the wavenumber ($k_j = (2j - 1)\pi/2L$). The wavenumber is related to the natural frequency as $\omega_j = ck_j$. After substituting for Eq. (4), Eq. (3) can be written as,

$$\begin{aligned} \sum_{j=1}^n \frac{\ddot{\eta}_j(t)}{\omega_j} \cos(k_j z) + \frac{\gamma \bar{p}}{\bar{\rho}c} \sum_{j=1}^n \eta_j(t) k_j \cos(k_j z) \\ = \frac{\gamma - 1}{\bar{p}} \dot{Q}' \delta(z - z_f). \end{aligned} \quad (5)$$

By integrating Eq. (5) over the volume of the combustor, after computing the inner product along each of the basis functions, we obtain

$$\frac{\ddot{\eta}_j(t)}{\omega_j} + ck_j \eta_j(t) = \frac{2(\gamma - 1)}{L\bar{p}} \int_0^L \dot{Q}' \delta(z - z_f) \cos(k_j z) dz. \quad (6)$$

Here, we choose the number of eigenmodes to be $j = 1$, which is adequate for analysing the characteristics of the transition discovered in the experiments conducted in the current study. Further, the observed dynamics in the combustors is a result of nonlinear response of the flame to the fluctuations in the acoustic field. Therefore, \dot{Q}' can be expressed as a nonlinear function of η and $\dot{\eta}$. Thus, Eq. (6) reduces to the equation of a self-excited harmonic oscillator, expressed as

$$\ddot{\eta} + \omega^2 \eta = f(\eta, \dot{\eta}), \quad (7)$$

where, $f(\eta, \dot{\eta}) = f(\dot{Q}') - \alpha \dot{\eta}$ is the nonlinear driving term. An extra term $\alpha \dot{\eta}$ is added to take acoustic damping into account (α is the damping coefficient)⁴². Thus, the source term $f(\eta, \dot{\eta})$ represents the nonlinear damping and driving behaviour of the oscillator. Further, $f(\eta, \dot{\eta})$ can be expanded with nonlinear terms such that Eq. (7) represents a Hopf bifurcation to thermoacoustic oscillations⁴³. The modified form of Eq. (7) is given as,

$$\ddot{\eta} + (\mu_2 \eta^2 - \mu_0) \dot{\eta} + \omega^2 \eta = 0, \quad (8)$$

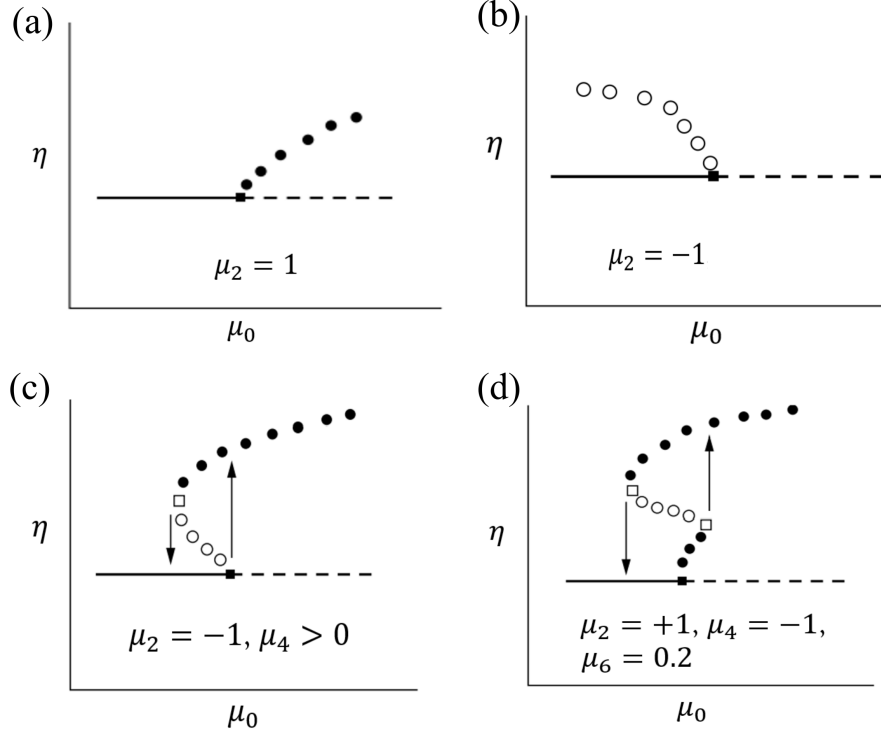


FIG. 6. Representation of the types of bifurcation obtained by augmenting the driving term $\dot{\eta}$ of Eq. (9) with the higher order nonlinear terms. **(a)** Supercritical Hopf bifurcation with a single stable branch of LCO. **(b)** Subcritical Hopf bifurcation with a single unstable LCO branch. **(c)** Subcritical Hopf bifurcation to a stable LCO branch. **(d)** Secondary bifurcation depicting a supercritical followed by an abrupt secondary transition to a high amplitude stable LCO. Open circles represent the unstable solutions, and the solid circles represent the stable solutions. This figure is reproduced with permission from Ananthkrishnan *et al.*³⁶

where μ_0 is the control parameter and μ_2 is the coefficient of the second order nonlinear term. Equation 8 also represents the Van der Pol oscillator, which is a paradigm for systems exhibiting limit cycle oscillations⁴⁴. When μ_2 is positive, we obtain a stable limit cycle branch denoting a supercritical Hopf bifurcation (refer to Fig. 6a). When μ_2 is negative, we obtain an unstable subcritical limit cycle branch (refer to Fig. 6b). The nonlinear coefficients associated with the driving term $\dot{\eta}$ in Eq. (8) can be augmented with higher order nonlinear coefficients to produce multiple limit cycle branches³⁶. This augmentation helps represent the multiple high amplitude limit cycle oscillations (LCO) in thermoacoustic systems¹⁶.

Therefore, we modify Eq. (8) as,

$$\ddot{\eta} + (\mu_6\eta^6 + \mu_4\eta^4 + \mu_2\eta^2)\dot{\eta} - \mu_0\dot{\eta} + \omega^2\eta = 0, \quad (9)$$

where μ_4 and μ_6 are the coefficients of the higher order nonlinear terms. By fixing $\mu_2 = -1$, $\mu_4 > 0$ and $\mu_6 = 0$, we obtain an unstable LCO branch followed by a stable LCO branch representing a subcritical Hopf bifurcation (Fig. 6c). Similarly by fixing $\mu_2 > 0$, $\mu_4 < 0$ and $\mu_6 > 0$, we obtain a secondary bifurcation as shown in Fig. 6d^{16,36}. Thus, from Fig. 6, we note that the coefficients of the nonlinear terms govern the stability and the amplitude of the LCO branches in the bifurcation curve.

Now, the dynamics of the canard explosion is such that the amplitude of the system becomes highly sensitive to a narrow range of parameters near the bifurcation regime. To achieve this, we reduce the magnitude of the coefficients of all the nonlinear terms ($\mu_6\eta^6 + \mu_4\eta^4 + \mu_2\eta^2$). Therefore, we couple all the nonlinear coefficients with a constant $\epsilon \ll 1$, reducing the strength of nonlinearity associated with the nonlinear terms. Such systems with reduced strength of nonlinearity are referred to as weakly nonlinear oscillators⁸. The modified equation with the coupling term ϵ is written as,

$$\ddot{\eta} + \epsilon (\mu_6\eta^6 + \mu_4\eta^4 + \mu_2\eta^2)\dot{\eta} - \mu_0\dot{\eta} + \omega^2\eta = 0. \quad (10)$$

To visualise the effect of the magnitude of ϵ , we obtain the dynamics of the amplitude-envelope of the oscillations from the harmonic oscillator Eq. (10), using the method of averaging^{8,16,45}. We substitute the acoustic variable to be of the form $\eta(t) = A(t)\cos[\omega t + \Omega(t)]$. Here, $A(t)$ and $\Omega(t)$ represent the amplitude-envelope and its phase, respectively. The evolution time scale of $A(t)$ and $\Omega(t)$ is much slower than the faster times scale of system $2\pi/\omega$. Thus, after substituting $\eta(A, \Omega)$ and averaging Eq. (10) over the faster time scale $2\pi/\omega$ ^{16,45}, the dynamics of the amplitude-envelope of the oscillations is obtained as,

$$\dot{A} = \frac{\mu_0}{2}A - \epsilon \left(\frac{\mu_2}{8}A^3 + \frac{\mu_4}{165}A^5 + \frac{5\mu_6}{128}A^7 \right). \quad (11)$$

We note that the evolution of the amplitude-envelope is a function $\dot{A} = f(\mu_0, A) - f(A^3, A^5, A^7)$, which is dependent on the control parameter μ_0 and the damping term $f(A^3, A^5, A^7)$. The nonlinear damping term $f(A^3, A^5, A^7)$ is in turn a function of the higher order terms $f(A^3)$, $f(A^5)$ and $f(A^7)$. The solutions for Eq. (11) are computed as $\dot{A} = 0$, which are obtained by balancing $f(\mu_0, A) = f(A^3, A^5, A^7)$ ⁸.

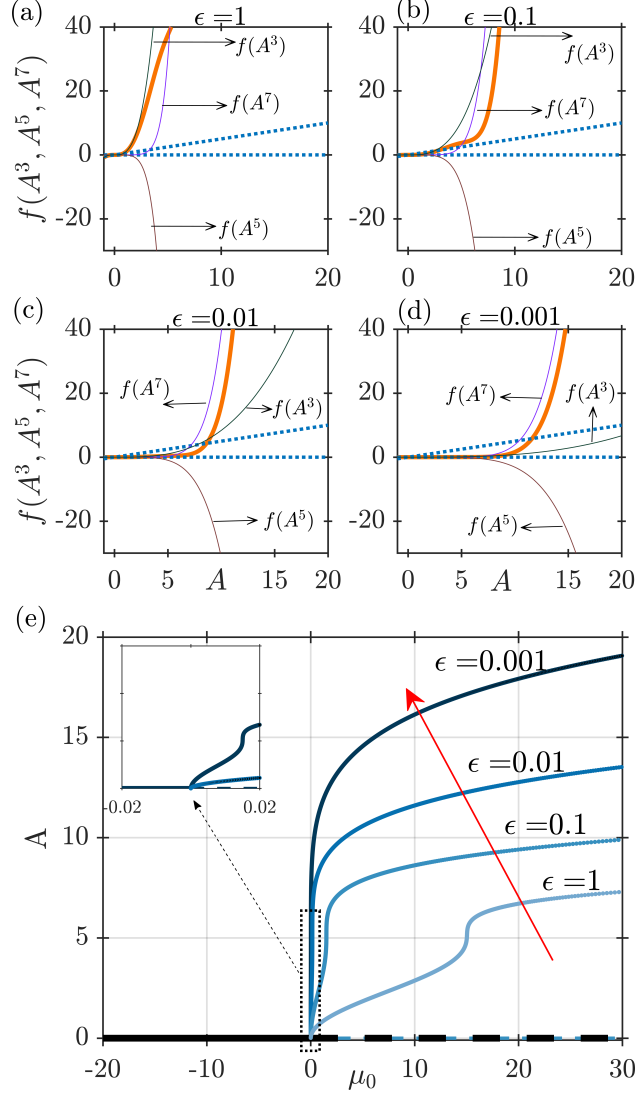


FIG. 7. **(a-d)** Representation of the effects of ϵ on the evolution of the solutions for Eq. (11), which is of the form $\dot{A} = f(\mu_0, A) - f(A^3, A^5, A^7)$. The ordinate denotes the values of $f(A^3, A^5, A^7)$ (thick orange curve), and the abscissa represents the values of A . The contributions from A^3 , A^5 , and A^7 are presented in the coloured thin solid curves. The dashed blue lines represent the control parameter curve $f(\mu_0, A)$ for $\mu_0 = 0$ and 1 . Geometrically, the solutions are the points of intersections of $f(A^3, A^5, A^7)$ and $f(\mu_0, A)$. **(e)** Bifurcation diagram to represent the effect of ϵ on the continuous secondary bifurcation curve obtained by fixing $\mu_2 = 6.7$, $\mu_4 = -0.5$, and $\mu_6 = 0.01$. The variation of μ_0 is shown on the abscissa and the solutions of Eq. (11) are shown on the ordinate. In the bifurcation diagram, thick lines are for stable solutions and the broken line is for unstable solutions. Notice that as ϵ is decreased from 1 to 0.001 , the range of parameters to reach the high amplitude oscillations after the bifurcation decreases to a very narrow span.

We proceed with considering a case of continuous secondary bifurcation obtained by setting $\mu_2 = 6.7$, $\mu_4 = -0.5$, and $\mu_6 = 0.01$. In Fig. 7(a-d), we represent the effect of ϵ on the evolution of solutions for Eq. (11). These solutions are, geometrically, the points of intersections of the curves $f(\mu_0, A)$ and $f(A^3, A^5, A^7)$. The thick orange line represents the curves for $f(A^3, A^5, A^7)$, which is a summation of contributions from $f(A^3)$, $f(A^5)$ and $f(A^7)$ represented with thin lines. The curves for $f(\mu_0, A)$, at $\mu_0 = 0$ and $\mu_0 = 1$, are shown in dotted blue lines. $f(\mu_0, A)$ is a line passing through the origin where μ_0 is its slope. Thus, we obtain several curves for $f(\mu_0, A)$ with varying slopes as we vary μ_0 as a control parameter, not shown here in the interest of space. From the figure 7(a,b), for the lower values of A , we see that the dynamics of the curve $f(A^3, A^5, A^7)$ (orange line) is mainly contributed from $f(A^3)$ and $f(A^5)$. We also note that as the value of ϵ decreases from 1 to 0.001, the absolute value of the functions ($|f(A^3)|$, $|f(A^5)|$, and $|f(A^7)|$) decreases, and their curves tend towards the abscissa (cf. Fig. 7a-d). The effect of the decrease in ϵ , for smaller amplitudes of A , is more pronounced on the lower order nonlinear terms $f(A^3)$ and $f(A^5)$ than on the highest order term $f(A^7)$ (cf. Fig. 7a-d). This influence of ϵ on the nonlinear terms collectively transforms the curve $f(A^3, A^5, A^7)$ to have lower slopes for an extended value of A (compare the orange lines of Fig. 7a-d). Thus, the transformation results in a scenario where we observe a rapid change in the value of solutions, the intersection of $f(A^3, A^5, A^7)$ and $f(\mu_0, A)$ (cf. Fig. 7c,d), for a minute change in the value of the parameter μ_0 in the range $|\mu_0| < 1$.

In Fig. 7(e), we plot the bifurcation curves for the cases of $\epsilon = 1, 0.1, 0.01$, and 0.001 obtained by varying the control parameters in the range of $-20 \leq \mu_0 \leq 30$. As ϵ is reduced, we notice that the bifurcation curve significantly steepens at the Hopf point $\mu_0 = 0$ (refer to Fig. 7e). In other words, the range of values of μ_0 to reach the saturation in the rise in amplitude decreases to a very narrow span (refer to the inset of Fig. 7e). The steepening of the transition curve occurs due to the higher reduction in the nonlinearity of lower-order nonlinear terms for lower amplitudes A , which otherwise form a continuous secondary bifurcation (refer to the curve $\epsilon = 1$, in Fig. 7). From figure. 7(a-d), we convey that the effect of ϵ is less on the highest-order nonlinear term η^6 when compared to the lower-order nonlinear terms in Eq. (10). Thus, the coupling term ϵ aids in obtaining a weakly nonlinear oscillator exhibiting a transition with a canard explosion at the Hopf point.

Further, utilising 4th order Runge-Kutta method, we numerically integrate Eq. (10) by

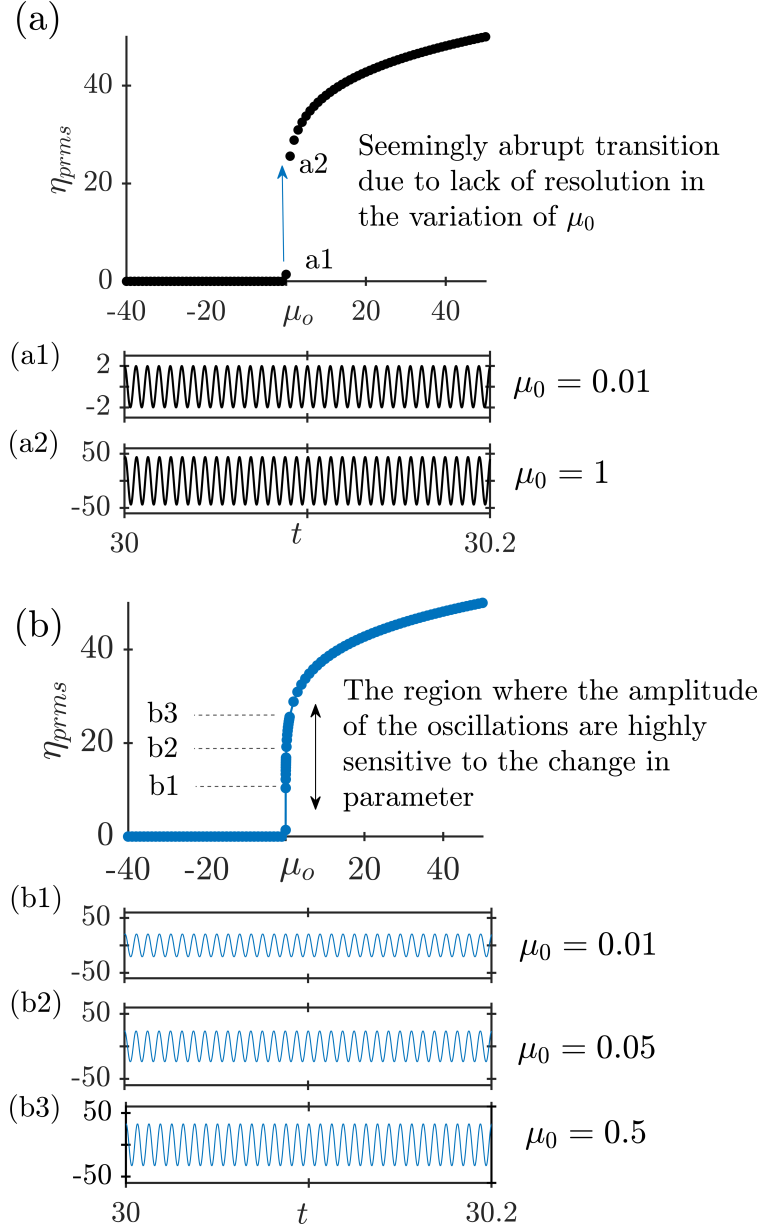


FIG. 8. Representation of the canard explosion by numerically integrating Eq. (10). The curves represent the variation of η_{rms} as a function of μ_o . When the control parameter μ_o is varied in steps of 1, we notice an abrupt jump in (a) the bifurcation diagram. The abrupt nature of the transition is due to a lack of resolution in the variation of the control parameter. The abrupt jump is also evident from the amplitude of the time series (a1) before and (a2) after the transition. However, when we vary the control parameter in finer steps, we have (b) stable dynamics at each of these finer steps. Thus, the model captures a rapid continuous transition (b1-b3), where the amplitude rises significantly with a negligible change in the control parameter μ_o .

fixing $\epsilon = 0.0001$ for a range of control parameter $-40 \leq \mu_0 \leq 50$ to obtain the bifurcation diagram. Figure 8a denotes the bifurcation curve when the control parameter μ_0 is varied in steps of 1. Since there is a significantly steeper rise, the transition appears to be abrupt at the Hopf point $\mu_0 = 0$ due to a weaker resolution in the variation of the control parameter. This seemingly abrupt transition is what we notice during the experiments as the system transitions to high-amplitude thermoacoustic instability (refer to Fig. 2a). We further illustrate that, by increasing the resolution at the canard explosion regime, the system exhibits the stable LCO at every small variation in μ_0 , implying a continuous sudden transition (refer to Fig. 8b).

Further, the experimental data on temperature fluctuations vary in correlation with the bursting amplitude at a slower time scale (refer to Fig. 5). This variation of the temperature fluctuations suggests that there is an additional parameter that fluctuates at a timescale slower than the thermoacoustic oscillations. When such an oscillating term is coupled with the driving term $\dot{\eta}$, the system exhibits bursting oscillations at the bifurcation regime³⁴. We illustrate the bursting phenomenon for an underlying canard explosion in the following subsection.

A. Bursting behaviour due to underlying canard explosion

The amplitude of the bursts corresponding to an underlying canard explosion is very high due to the sudden nature of the transition at the bifurcation regime. Experimentally, we observed that a system parameter (T') fluctuates at a slower time scale at the bifurcation regime of the canard explosion (refer to Fig. 5). Such parametric oscillations are also reported in past studies of thermoacoustic systems^{34,35}. Kasthuri, Unni, and Sujith³⁴ showed that the temperature close to the burner oscillates at a much slower time scale than the thermoacoustic oscillations during the state of bursting. In a swirl stabilized turbulent combustor, Hong *et al.*⁴⁶ showed that there is a fluctuation in the equivalence ratio during the state of large amplitude bursting. Tandon *et al.*³⁵ replicated the bursting dynamics of the low-turbulence systems using a phenomenological model containing slow-fast time scales. In line with the conjectures of these studies, one would intuitively expect large amplitude bursting oscillations in a system containing slow-fast time scales across the canard explosions. Inspired by these studies, we further illustrate the effect of the fluctuation of

the system parameter at the bifurcation regime of a canard explosion; for that, we couple the driving term $\dot{\eta}$ with a periodic oscillation of a very low frequency ω_q with a coupling strength of q . Thus, Eq. (10) is further modified as,

$$\begin{aligned} \ddot{\eta} + \epsilon (\mu_6 \eta^6 + \mu_4 \eta^4 + \mu_2 \eta^2) \dot{\eta} - \mu_0 \dot{\eta} \\ - [q \sin(\omega_q t) + \xi_m] \dot{\eta} + \omega^2 \eta + \xi_a = 0. \end{aligned} \quad (12)$$

The coupling is added with the multiplicative noise ξ_m to model the fluctuations associated with the driving as a result of the internal noise in the system⁴⁷. We also add additive white noise ξ_a to the Eq. (12) to incorporate the effect of turbulence⁴². Here, ξ is the white noise defined as $\langle \xi \xi_\tau \rangle = \Gamma \delta \tau$, where Γ is the noise intensity. The subscripts ‘ m ’ and ‘ a ’ denote the correspondence to multiplicative and additive noise, respectively.

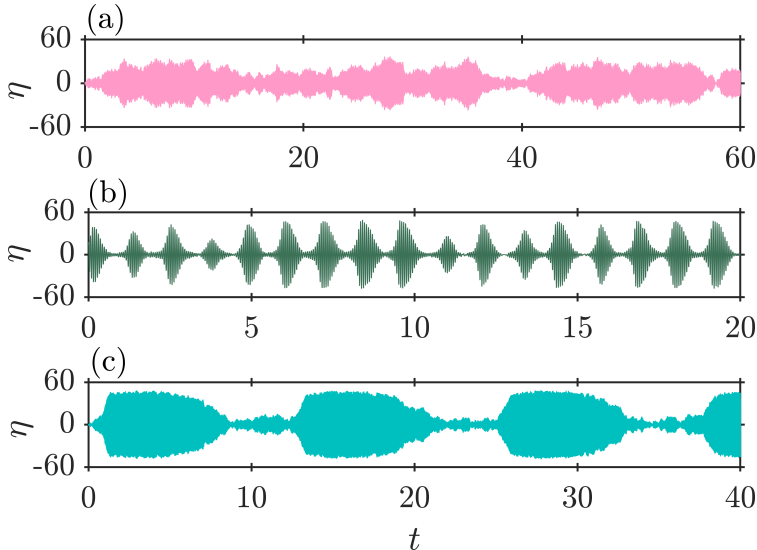


FIG. 9. Representation of the time series for bursting behaviour at the bifurcation regime of the canard explosion, obtained by numerical integration of Eq. (12). **(a)** Time series analogous to the bursting behaviour of a bluff body stabilized dump combustor. **(b)** Time series analogous to the bursting behaviour of a swirl stabilized dump combustor. **(c)** Time series analogous to the bursting behaviour of an annular combustor. We notice large amplitude bursts at the bifurcation regime due to the underlying canard explosion

The qualitative nature of the bursting behaviour obtained from the model for different types of combustors is represented in Fig. 9. At $\mu_0 = 0$, fixing $q = 0$, $\Gamma_a = 10^5$ and $\Gamma_m = 10^4$, we obtain the bursting behaviour that matches with the time series obtained from the bluff

body stabilized dump combustor (refer to Fig. 9a). The irregularity in the bursting pattern is due to the multiplicative noise ξ_m associated with the driving term $\dot{\eta}$. When we fix $\omega = 370$ rad/s, $\omega_q = 3$ rad/s, $q = 20$ rad/s, $\Gamma_a = 10^5$ and $\Gamma_m = 10^4$, we obtain a bursting pattern observed in the swirl stabilized dump combustor (refer to Fig. 9b).

Further, upon fixing $\omega = 370$, rad/s, $\omega_q = 0.5$ rad/s, $q = 20$ rad/s, $\Gamma_a = 10^7$ and $\Gamma_m = 10^5$, we obtain a bursting pattern observed in the annular combustor (refer to Fig. 9b). The coupling oscillation frequency ω_q for the case of an annular combustor is lesser than that of the swirler stabilized dump combustor. Hence, the bursts in the annular combustor are of longer duration. Thus, using these results from the model we illustrate that large amplitude bursts are observed in turbulent combustors when a system parameter fluctuates at the bifurcation regime of an underlying canard explosion.

V. CONCLUSIONS

In summary, we reported the experimental evidence for the occurrence of canard explosion in three different turbulent reactive flow systems—a bluff body and a swirl-stabilized dump combustor, and a swirl-stabilized annular combustor. The transition appears discontinuous when there is a lack of resolution in the variation of the control parameter. Though the rise in amplitude of the oscillations is steep in nature, unlike abrupt transitions, the canard explosion in this study exhibits no hysteresis. When such a transition involves a parameter fluctuation at the bifurcation regime, the system is bound to exhibit bursting behaviour with large amplitude bursts. We experimentally showed that the state of the bursting, in the regime of canard explosions, consists of very high amplitude fluctuations amidst low amplitude fluctuations.

We describe the transition via the canard explosion using the low-order model representing thermoacoustic systems. A continuous secondary bifurcation steepens at the bifurcation regime when the nonlinearity of the nonlinear damping in the model is reduced by coupling a small variable ϵ . In other words, the dynamics of the transition from stable operation to high amplitude oscillatory instability gets restricted to a very narrow range of control parameters, for the values of $\epsilon \ll 1$. For such a steepened transition, we conjecture that the system amplitude becomes highly sensitive to the change in control parameter at the bifurcation regime, thus giving rise to a scenario of large amplitude bursts.

Further, during the state of bursting, we observe a slow variation in the fluctuation of the exhaust gas temperature in correlation with the envelope of the acoustic pressure fluctuation. The temperature of the exhaust gas represents the flame temperature as well as the fluctuation in the heat release rate, which in turn governs the dynamics of the thermoacoustic oscillations. We convey that parameter fluctuation has a role in bursting behaviour in the regime of canard explosion, as explained using the low-order thermoacoustic model. A further study that consists of flow visualisation is required to differentiate the underlying flow physics between the canard explosions, abrupt transition and gradual bifurcation in turbulent thermoacoustic systems.

ACKNOWLEDGMENTS

We acknowledge the support from Mr Pruthiraj M., Mr Rohit R. and Mr Beeraiah T. for their useful discussions while conducting experiments. We also thank Ms Athira, Ms Ariakutty, Mr Thilagaraj S. and Mr Anand S. for their technical support in experiments. Ramesh S. Bhavi and Sivakumar S. are thankful to the Ministry of Education (MoE) for the research assistantship. R. I. Sujith thanks the IoE initiative (SP22231222CPETWOCTSHOC) and SERB/CRG/2020/003051 from the Department of Science and Technology for funding this work.

DATA AVAILABILITY

The data that support the findings of this study are available from the corresponding author upon reasonable request.

REFERENCES

- ¹R. I. Sujith and S. Pawar, *Thermoacoustic Instability: A Complex Systems Perspective*, Springer Series in Synergetics (Springer International Publishing, Cham, Switzerland, 2021).
- ²A. Hirschberg and S. W. Rienstra, *An Introduction to Aeroacoustics* (Eindhoven University of Technology, 2004).

- ³M. H. Hansen, “Aeroelastic instability problems for wind turbines,” *Wind Energy* **10**, 551–577 (2007).
- ⁴G. V. Parkinson, “Wind-induced instability of structures,” *Phil. Trans. Roy. Soc. Lon. A.* **269**, 395–409 (1971).
- ⁵T. C. Lieuwen, *Investigation of combustion instability mechanisms in premixed gas turbines* (Ph. D. thesis, Georgia Institute of Technology, Georgia, United States, 1999).
- ⁶R. S. Brown, R. Dunlap, S. W. Young, and R. C. Waugh, “Vortex shedding as a source of acoustic energy in segmented solid rockets,” *Journal of Spacecraft and Rockets* **18**, 312–319 (1981).
- ⁷T. C. Lieuwen, “Experimental investigation of limit-cycle oscillations in an unstable gas turbine combustor,” *J. Propuls. Power* **18**, 61–67 (2002).
- ⁸S. H. Strogatz, *Nonlinear Dynamics and Chaos, With Applications to Physics, Biology, Chemistry, and Engineering* (CRC press, Boca Raton, Florida, 2018).
- ⁹S. Etikyala and R. I. Sujith, “Change of criticality in a prototypical thermoacoustic system,” *Chaos* **27**, 023106 (2017).
- ¹⁰P. Subramanian, S. Mariappan, R. I. Sujith, and P. Wahi, “Bifurcation analysis of thermoacoustic instability in a horizontal Rijke tube,” *Int. J. Spray Combust. Dyn.* **2**, 325–355 (2010).
- ¹¹H. Gotoda, H. Nikimoto, T. Miyano, and S. Tachibana, “Dynamic properties of combustion instability in a lean premixed gas-turbine combustor,” *Chaos* **21**, 013124 (2011).
- ¹²S. Mondal, V. R. Unni, and R. I. Sujith, “Onset of thermoacoustic instability in turbulent combustors: an emergence of synchronized periodicity through formation of chimera-like states,” *J. Fluid Mech.* **811**, 659–681 (2017).
- ¹³V. Nair, G. Thampi, and R. I. Sujith, “Intermittency route to thermoacoustic instability in turbulent combustors,” *J. Fluid Mech.* **756**, 470–487 (2014).
- ¹⁴I. Pavithran, V. R. Unni, A. J. Varghese, R. I. Sujith, A. Saha, N. Marwan, and J. Kurths, “Universality in the emergence of oscillatory instabilities in turbulent flows,” *EPL* **129**, 24004 (2020).
- ¹⁵S. Singh, A. Roy, K. V. Reeja, A. Nair, S. Chaudhuri, and R. I. Sujith, “Intermittency, secondary bifurcation and mixed-mode oscillations in a swirl-stabilized annular combustor: Experiments and modeling,” *J. Eng. Gas Turbines Power.* **143**, 051028 (2021).

- ¹⁶R. S. Bhavi, I. Pavithran, A. Roy, and R. I. Sujith, “Abrupt transitions in turbulent thermoacoustic systems,” *J. Sound Vib.* **547**, 117478 (2023).
- ¹⁷A. Joseph, I. Pavithran, and R. I. Sujith, “Explosive synchronization in a turbulent reactive flow system,” *Chaos* **34**, 021105 (2024).
- ¹⁸P. Kumar, D. K. Verma, P. Parmananda, and S. Boccaletti, “Experimental evidence of explosive synchronization in mercury beating-heart oscillators,” *Phys. Rev. E* **91**, 062909 (2015).
- ¹⁹Y. Zou, T. Pereira, M. Small, Z. Liu, and J. Kurths, “Basin of attraction determines hysteresis in explosive synchronization,” *PRL* **112**, 114102 (2014).
- ²⁰M. Brøns and K. Bar-Eli, “Canard explosion and excitation in a model of the Belousov-Zhabotinsky reaction,” *J. Phys. Chem.* **95**, 8706–8713 (1991).
- ²¹M. Krupa and P. Szmolyan, “Relaxation oscillation and canard explosion,” *J. Differ. Equ.* **174**, 312–368 (2001).
- ²²J. Rankin, M. Desroches, B. Krauskopf, and M. Lowenberg, “Canard cycles in aircraft ground dynamics,” *Nonlinear Dyn.* **66**, 681–688 (2011).
- ²³J. Moehlis, “Canards for a reduction of the Hodgkin-Huxley equations,” *J. Math. Biol.* **52**, 141–153 (2006).
- ²⁴B. Deng, “Food chain chaos with canard explosion,” *Chaos* **14**, 1083–1092 (2004).
- ²⁵F. Marino, M. Ciszak, S. F. Abdalah, K. Al-Naimee, R. Meucci, and F. T. Arecchi, “Mixed-mode oscillations via canard explosions in light-emitting diodes with optoelectronic feedback,” *Phys. Rev. E* **84**, 047201 (2011).
- ²⁶C. Børgers, *An introduction to modeling neuronal dynamics*, Vol. 66 (Springer, 2017).
- ²⁷M. Diener, “The canard unchained or how fast/slow dynamical systems bifurcate,” *Math. Intell.* **6**, 38–49 (1984).
- ²⁸X. Han and Q. Bi, “Slow passage through canard explosion and mixed-mode oscillations in the forced Van der Pol’s equation,” *Nonlinear Dyn.* **68**, 275–283 (2012).
- ²⁹M. Desroches, T. J. Kaper, and M. Krupa, “Mixed-mode bursting oscillations: Dynamics created by a slow passage through spike-adding canard explosion in a square-wave burster,” *Chaos* **23** (2013).
- ³⁰B. T. Zinn, “Pulse combustion applications: Past, present and future,” in *Unsteady Combustion*, edited by F. Culick, M. V. Heitor, and J. H. Whitelaw (Springer Netherlands, Dordrecht, 1996) pp. 113–137.

- ³¹T. H. Chen, L. P. Goss, D. D. Trump, and W. J. Schmoll, “Studies of a turbulent premixed flame using CARS-LDV diagnostics,” *J. Propuls. Power* **6**, 106–114 (1990).
- ³²I. Pavithran, P. R. Midhun, and R. I. Sujith, “Tipping in complex systems under fast variations of parameters,” *Chaos* **33** (2023).
- ³³E. M. Izhikevich, “Neural excitability, spiking and bursting,” *Int. J. Bifurc. Chaos* **10**, 1171–1266 (2000).
- ³⁴P. Kasthuri, V. R. Unni, and R. I. Sujith, “Bursting and mixed mode oscillations during the transition to limit cycle oscillations in a matrix burner,” *Chaos* **29**, 043117 (2019).
- ³⁵S. Tandon, S. A. Pawar, S. Banerjee, A. J. Varghese, P. Durairaj, and R. I. Sujith, “Bursting during intermittency route to thermoacoustic instability: Effects of slow–fast dynamics,” *Chaos* **30**, 103112 (2020).
- ³⁶N. Ananthkrishnan, K. Sudhakar, S. Sudershan, and A. Agarwal, “Application of secondary bifurcations to large-amplitude limit cycles in mechanical systems,” *J. Sound Vib.* **215**, 183–188 (1998).
- ³⁷F. Nicoud and K. Wiecek, “About the zero Mach number assumption in the calculation of thermoacoustic instabilities,” *Int. J. Spray Combust. Dyn.* **1**, 67–111 (2009).
- ³⁸K. Balasubramanian and R. I. Sujith, “Thermoacoustic instability in a Rijke tube: Non-normality and nonlinearity,” *Phys. Fluids* **20**, 044103 (2008).
- ³⁹K. McManus, T. Poinot, and S. M. Candel, “A review of active control of combustion instabilities,” *Prog. Energy Combust. Sci.* **19**, 1–29 (1993).
- ⁴⁰T. C. Lieuwen, *Unsteady Combustor Physics*, 2nd ed. (Cambridge University Press, Cambridge, 2021).
- ⁴¹M. E. Lores and B. T. Zinn, “Nonlinear longitudinal combustion instability in rocket motors,” *Combust. Sci. and Tech.* **7**, 245–256 (1973).
- ⁴²N. Noiray, “Linear growth rate estimation from dynamics and statistics of acoustic signal envelope in turbulent combustors,” *J. Eng. Gas Turbines Power.* **139** (2017).
- ⁴³G. Bonciolini, A. Faure-Beaulieu, C. Bourquard, and N. Noiray, “Low order modelling of thermoacoustic instabilities and intermittency: Flame response delay and nonlinearity,” *Combust. Flame* **226**, 396–411 (2021).
- ⁴⁴N. Minorsky, *Nonlinear Oscillations* (D. Van Nostrand company, Inc., Princeton, New Jersey, 1962).

- ⁴⁵A. Balanov, N. Janson, D. Postnov, and O. Sosnovtseva, *Synchronization: From Simple to Complex*, Springer Series in Synergetics (Springer, Heidelberg, Germany, 2009).
- ⁴⁶J. G. Hong, K. C. Oh, U. D. Lee, and H. D. Shin, “Generation of low-frequency alternative flame behaviors in a lean premixed combustor,” *Energy Fuels* **22**, 3016–3021 (2008).
- ⁴⁷P. Clavin, J. Kim, and F. Williams, “Turbulence-induced noise effects on high-frequency combustion instabilities,” *Combust. Sci. and Tech.* **96**, 61–84 (1994).